

Inferring the magnetic field vector in the quiet Sun

II. Interpreting results from the inversion of Stokes profiles

J.M. Borrero¹ and P. Kobel²

¹ Kiepenheuer-Institut für Sonnenphysik, Schöneckstr. 6, D-79110, Freiburg, Germany. e-mail: borrero@kis.uni-freiburg.de

² Max-Planck Institut für Sonnensystemforschung, Max-Planck Str. 2, Katlenburg-Lindau, 37191, Germany. e-mail: kobel@mps.mpg.de

Received / Accepted

ABSTRACT

In a previous paper, we argued that the inversion of Stokes profiles applied to spectropolarimetric observations of the solar internetwork yield unrealistically large values of the inclination of the magnetic field vector (γ). This is because photon noise in Stokes Q and U are interpreted by the inversion code as valid signals, that leads to an overestimation of the transverse component B_{\perp} , thus the inclination γ . However, our study was based on the analysis of linear polarization signals that featured only uncorrelated noise. In this paper, we develop this idea further and study this effect in Stokes Q and U profiles that also show correlated noise. In addition, we extend our study to the three components of the magnetic field vector, as well as the magnetic filling factor α . With this, we confirm the tendency to overestimate γ when inverting linear polarization profiles that, although non-zero, are still below the noise level. We also establish that the overestimation occurs mainly for magnetic fields that are nearly vertical $\gamma \lesssim 20^\circ$. This indicates that a reliable inference of the inclination of the magnetic field vector cannot be achieved by analyzing only Stokes I and V . In addition, when inverting Stokes Q and U profiles below the noise, the inversion code retrieves a randomly uniform distribution of the azimuth of the magnetic field vector ϕ . To avoid these problems, we propose only inverting Stokes profiles for which the linear polarization signals are sufficiently above the noise level. However, this approach is also biased because, in spite of allowing for a very accurate retrieval of the magnetic field vector from the selected Stokes profiles, it selects only profiles arising from highly inclined magnetic fields.

Key words. Magnetic fields – Sun: photosphere – Sun: surface magnetism – Stars: magnetic field

1. Introduction

Spectropolarimetry, which is the study of the polarization properties of the light observed in spectral lines, is the most developed and widely used tool for retrieving the magnetic properties of the solar plasma and other astrophysical objects (Stenflo 2002; Mathys 2002 and references therein). The inference of the magnetic field vector from spectropolarimetric observations is performed through the inversion of the radiative transfer equation for polarized light (del Toro Iniesta 2003a; Bellot Rubio 2004; Ruiz Cobo 2007). However, as the module of the magnetic field vector decreases, the observed signals disappear below the level of the photon noise, making the inference of the magnetic field very difficult and plagued with problems and uncertainties. This is, for instance, the case for the areas on the solar surface referred to as the *solar internetwork*. Here, the polarization signals are so weak that for a long time the internetwork was thought to be void of magnetic fields.

With the advancements in the sensitivity of the polarimeters and the higher spatial resolution of the observations achievable with adaptive-optic systems and large-aperture telescopes, polarization signals are now routinely detected everywhere in the internetwork (Lites et al. 1996). This demonstrates that these regions are truly

pervaded by magnetic fields. Unfortunately, the signals are barely above the noise level, thus it has not yet been possible to fully characterize the magnetic field vector in these regions. This has led to a long-standing controversy about the distribution of the module of the magnetic field vector in the internetwork (Domínguez Cerdeña et al. 2003; Socas-Navarro & Lites 2004; Sánchez Almeida 2005; Martínez González et al. 2006; Asensio Ramos et al. 2007; López Ariste et al. 2007; Socas-Navarro et al. 2008; see also references therein).

More recently, further discrepancies have emerged about the angular distribution of the magnetic field vector (Lites et al. 2007, 2008; Orozco Suárez et al. 2007a, 2007b; Martínez González et al. 2008; Asensio Ramos 2009; Stenflo 2010; Ishikawa & Tsuneta 2011; Borrero & Kobel 2011). In Borrero & Kobel (2011; hereafter referred to as paper I), we argued that the photon noise leads to a systematic overestimation of the inclination of the magnetic field vector. We reached this conclusion because when employing only vertical magnetic fields to synthesize Stokes profiles, these could be retrieved as highly inclined ones due to the sole effect of the photon noise. Since those tests were carried out with vertical magnetic fields, the linear polarization signals (Stokes Q and U) were zero. This limits the validity of the tests, as the inversion

code analyzes only linear polarization profiles featuring uncorrelated noise. It is therefore worth considering the case where small linear-polarization signals (due to non-vertical magnetic fields) can be hidden below the noise. This introduces correlations that could be employed by the inversion algorithms to retrieve useful information about the inclination of the magnetic field vector. This paper is devoted to addressing this particular situation. To this end, we employ uniform distributions of the magnetic field vector (Section 2) to produce a large database of Stokes profiles. Therefore, unlike paper I, the resulting Stokes profiles will have non-zero linear polarization profiles. After adding noise to these profiles, we apply an inversion algorithm (Section 3) that attempts to retrieve the original distribution of the magnetic field vector. Our results are described in Sections 4 and 5. Section 6 summarizes our findings.

2. Synthesis with uniform distributions

To study the effect of the photon noise and selection criterion, we performed several numerical experiments employing a probability distribution function that is parametrized by the physical parameters of a Milne-Eddington atmosphere (ME). These physical parameters are denoted as \mathbf{X}

$$\mathbf{X} = [\mathbf{B}, \alpha, V_{\text{los}}, \mathbf{T}], \quad (1)$$

where \mathbf{B} refers to the magnetic field vector, α is the so-called magnetic filling factor and denotes the fractional area within the pixel that is occupied by magnetized plasma, V_{los} is the line-of-sight component of the velocity vector, and, finally, the vector \mathbf{T} considers all thermodynamic quantities (source function, Doppler width, and so forth). More details about these parameters and the Milne-Eddington approximation can be found in Landi Degl’Innocenti (1992) and del Toro Iniesta (2003b). Here we write the probability distribution function for the ME parameters \mathbf{X} in the form

$$\mathcal{P}(\mathbf{X})d\mathbf{X} = \mathcal{P}_1(\mathbf{B}, \alpha)\mathcal{P}_2(\mathbf{T}, V_{\text{los}})d\mathbf{B}d\alpha d\mathbf{T}dV_{\text{los}}, \quad (2)$$

where the thermodynamic and kinematic parameters, \mathbf{T} and V_{los} , are assumed to be statistically independent of the magnetic ones \mathbf{B} and α . The distribution function of the former parameters $\mathcal{P}_2(\mathbf{T}, V_{\text{los}})$ is the one obtained from the inversion of map A in Borrero & Kobel (2011), so that we employ values that are representative of the quiet Sun. The term that contains the properties of the magnetic field, $\mathcal{P}_1(\mathbf{B}, \alpha)$, has been modeled as a slightly-modified uniform distribution, expressed as

$$\mathcal{P}_1(\mathbf{B}, \alpha)d\mathbf{B}d\alpha = \frac{1}{2\pi^2 B_0} H(B - B_0) dB d\gamma d\phi d\alpha, \quad (3)$$

which gives the probability of finding a magnetic field vector \mathbf{B} whose module is between B and $B + dB$, whose inclination (with respect to the observer’s line-of-sight) is between γ and $\gamma + d\gamma$, and whose azimuth (in the plane perpendicular to the observer’s line-of-sight) is between

ϕ and $\phi + d\phi$. On the right-hand-side of this equation, the term $H(B - B_0)$ also refers to the complementary Heaviside function

$$H(B - B_0) = \begin{cases} 1, & \text{if } B < B_0 \\ 0, & \text{if } B > B_0 \end{cases}, \quad (4)$$

where B_0 is taken as $B_0 = 200$ G in order to make our experiment representative of weak field regions in the solar surface. In addition to the value of B_0 , we do not make any further attempts to employ a more realistic model for the solar internetwork since our aim is not to investigate particular distribution functions, but rather to study the effect of the inversion, photon noise and selection criteria in the inference of the magnetic field vector in a general way.

Once we have the probability distribution function given by Eqs. 2-3-4, we solve the radiative transfer equation in order to create a large database ($= 2 \times 10^6$) of synthetic/theoretical Stokes profiles of the Fe I 6302.5 Å ($g_{\text{eff}} = 2.5$) spectral line. The effective Landé factor of the atomic transition calculated under the LS coupling scheme is indicated by g_{eff} . The Stokes profiles are synthesized with the VFISV (Very Fast Inversion of the Stokes Vector) inversion code of Borrero et al. (2010). To these profiles, photon noise is added as a normally distributed random variable with a standard deviation of $\sigma = 10^{-3}, 3 \times 10^{-4}$. These two values mimic the noise levels of maps A and C in Borrero & Kobel (2011). Once the noise is added, the resulting Stokes profiles are taken as real observations and inverted in order to retrieve the original atmospheric parameters \mathbf{X} . This step is described in the next section.

3. Inversions of synthetic Stokes profiles

The Stokes profiles for Fe I 6302.5 Å synthesized in the previous section are now inverted with the same VFISV code, but now running in inversion mode instead of synthesis mode. At the start, VFISV solves the radiative transfer equation for polarized light in the Milne-Eddington (ME) approximation using a set of initial values for the physical parameters: \mathbf{X}_0 . The solution of the radiative transfer equation yields theoretical or synthetic Stokes profiles that are compared to the ones synthesized in the previous section (those where photon noise had been added). The initial values of \mathbf{X}_0 are then iteratively modified until the best possible fit between the theoretical/synthetic and observed Stokes vector is reached. The final \mathbf{X}_f that achieves the best fit is then assumed to be the real one present in the solar atmosphere. In this work we will focus mainly on the magnetic field vector \mathbf{B} and magnetic filling factor α . For more details about how the inversion is performed, additional free parameters of the inversion, and treatment of the filling factor, we refer the reader to Borrero et al. (2010) and Borrero & Kobel (2011; paper I). We note that, since we are using the same type of atmospheric model in the synthesis and inversion (ME atmospheres), the experiments carried out in this paper do not address the systematic errors introduced by the choice of the wrong atmospheric model, such as those introduced when inverting asymmetric Stokes profiles using a ME

atmospheric model¹.

Once B , γ , ϕ and α had been retrieved from each Stokes profiles of the original database, we applied two different selection criteria. In the first criteria, we select for the analysis profiles in the database where the maximum of the absolute value (for all wavelengths) in *any* of the polarization signals (Stokes Q , U , or V) is larger than 4.5 times the noise level $\max|Q(\lambda), U(\lambda), V(\lambda)| \geq 4.5\sigma$. This is equivalent to selecting pixels where the signal-to-noise ratio (S/R) in the polarization profiles is 4.5 or better, i.e., $S/R \geq 4.5$. Hereafter we refer to this criteria as S/R_{quv} . In the second criteria we select those profiles within the database where the maximum of the absolute value (for all wavelengths) in the linear polarization signals (Stokes Q , U) is larger than 4.5 times the noise level $\max|Q(\lambda), U(\lambda)| \geq 4.5\sigma$. This criteria will be referred to as S/R_{qu} .

The reason behind the choice of these two different selection criteria is the following. The first criterion (selection of profiles where $S/R_{\text{quv}} \geq 4.5$) was adopted so we can draw parallelisms with both the results presented in paper I and Orozco Suárez et al. (2007a, 2007b). Owing to the intrinsic amplitude of Stokes Q , U , and V , this criterion selects mostly pixels where only the circular polarization V possesses a $S/R \geq 4.5$. The actual percentages depend on the distribution of the magnetic field vector and the level of noise. For instance, taking a uniform distribution of B , γ , and ϕ (Equation 3) and considering a noise-level of $\sigma = 10^{-3}$, only 21.2 % of the profiles selected with the S/R_{quv} -criterion possess linear polarization signals (Stokes Q and U) with peak-values above 4.5σ . In the remaining 78.8 % of the profiles, only Stokes V is above 4.5σ . The 21.2 % increases up to 39.1 % when considering a noise level of $\sigma = 3 \times 10^{-4}$. In paper I, the maps that had equivalent levels of noise featured different percentages of profiles: in the map with $\sigma = 10^{-3}$, only about 8.8 % of the profiles selected with the S/R_{quv} -criterion had linear polarization profiles above 4.5σ . This number increased to 38.8 % in the map with $\sigma = 3 \times 10^{-4}$. As already demonstrated in that paper (see also Martínez-González et al. 2011), the inversion of profiles selected with the S/R_{quv} -criterion yields values for the inclination of the magnetic field vector, γ , that are largely overestimated. This happens because most of the Stokes profiles have linear polarization signals that are either below or close to the noise level. This effect decreases as the noise in the polarization profiles goes down so that the linear polarization signal rises above the noise. However, since both Stokes Q and U remain below 10^{-4} for transverse fields up to $B_{\perp} \approx 20 - 30$ G, the overestimation in the inclination remains significant even at such low levels of noise.

In paper I, we proposed, as an alternative solution, selecting for the inversion only pixels where the peak in the Q or U signals is at least 4.5 times higher than the noise

i.e., where the S/R is higher than 4.5 in linear polarization. We also followed this approach in applying the second criterion (see also Asensio Ramos 2009). In paper I, we anticipated that this approach has the advantage of retrieving more trustworthy values of γ , B_{\perp} , and B but we did not quantify it.

With the results from the selected profiles using the aforementioned selection criteria, we constructed histograms for the magnetic field strength B , the inclination of the magnetic field vector with respect to the observer's line-of-sight γ , the projection of the magnetic field vector along the observer's line-of-sight $B_{\parallel} = B \cos \gamma$, the projection of the magnetic field vector along the perpendicular direction to the observer's line-of-sight: $B_{\perp} = B \sin \gamma$; azimuthal angle of the magnetic field vector in the plane perpendicular to the observer: ϕ , and finally the magnetic filling factor α . Results for $\sigma = 10^{-3}$ and S/R_{quv} are displayed in Figure 1, whereas Figure 2 presents the results for $\sigma = 3 \times 10^{-4}$ and S/R_{quv} . Likewise, Figures 3 and 4 present the results for these same levels of noise, respectively, but employing the S/R_{qu} selection criterion. The panels in each of these four figures correspond to the following histograms: **a)** the component of the magnetic field vector along the observer's line-of-sight B_{\parallel} ; **b)** the component of the magnetic field vector perpendicular the observer's line-of-sight B_{\perp} ; **c)** the module of the magnetic field vector B ; **d)** the inclination of the magnetic field vector with respect to the observer's line-of-sight γ ; **e)** the azimuthal angle of the magnetic field vector in the plane perpendicular to the observer's line-of-sight ϕ ; and finally **f)**-panels for the magnetic filling factor α . In all panels, solid-black lines represent the initial distribution employed in the synthesis of the Stokes profiles (see Eqs. 2-4) including all 2×10^6 Stokes profiles of the distribution. As required, the distributions for B , γ , ϕ , and α are uniform (equal probabilities). We note that this is not the case for $B_{\parallel} = B \cos \gamma$ and $B_{\perp} = B \sin \gamma$ because the cosine and sine functions introduce non-uniformities in the distribution. In addition, dashed-black lines represent the original distribution of the physical parameters but considering only the profiles that are selected with corresponding selection criteria, namely S/R_{quv} in Figs. 1-2, and S/R_{qu} in Figs. 3-4. Finally, the solid-red lines present the distributions inferred from the inversion of the Stokes profiles but employing the same Stokes profiles that were used to construct the dashed-black histograms. In the following we comment on some general features that will assist us in interpreting our results:

- The area under the solid-black curve is always one, while the area under the dashed-black and solid-red curves are both normalized to the quotient of the number of profiles selected with each particular criteria and the total number of profiles synthesized (2×10^6). Therefore, one can interpret the difference between the solid-black and dashed-black curves as the loss of information caused by selection criterion, whereas the differences between dashed-black and solid-red are caused by the inversion algorithm.
- If the solid-red curve lies below the dash-black one for a given interval of the physical parameter (e.g.

¹ Other sources of systematic errors that are not being considered, as they are beyond the scope of our study, are the effects of the spatial resolution, spectral resolution, etcetera. For instance, Borrero et al. (2007) carried out such a study for the particular case of the Helioseismic and Magnetic Imager (HMI) instrument.

$\Delta\gamma$), it means that the number of Stokes profiles that were synthesized employing that range of values (e.g. $\Delta\gamma$) are underestimated by the inversion. Likewise, whenever the solid-red curve lies above the dash-black one for a given interval, the inversion overestimates the number of Stokes profiles that were synthesized employing the range of values of the physical parameter given by the same interval.

- The area under the dashed-black lines in each panel increases as the noise level decreases. This can be realized by comparing Figure 1 ($\sigma = 10^{-3}$) with Figure 2 ($\sigma = 3 \times 10^{-4}$), and also comparing Figure 3 ($\sigma = 10^{-3}$) with Figure 4 ($\sigma = 3 \times 10^{-4}$). This happens as a consequence of a larger number of Stokes profiles fulfilling the requirement imposed by a given selection criterion when the noise is reduced. Since the S/R_{qu} is more stringent than S/R_{quv} (because linear polarization signals are usually much weaker than the circular polarization signals), the area under the dashed-black curves is of course much larger in Figs. 1-2 than Figs. 3-4.

4. Discussion

We now discuss qualitatively the effects of photon noise and selection criteria for each physical parameter individually. We first introduce the approximate dependences of the Stokes profiles on the three spherical coordinates of the magnetic field vector (B , γ , ϕ) and the magnetic filling factor α , in the weak field approximation (Landi Degl’Innocenti 1992)

$$\begin{aligned} V &\propto \alpha B \cos \gamma \\ Q &\propto \alpha B^2 \sin^2 \gamma \cos 2\phi \\ U &\propto \alpha B^2 \sin^2 \gamma \sin 2\phi \end{aligned} \quad (5)$$

4.1. Line-of-sight component of the magnetic field: B_{\parallel}

As mentioned in the previous Section, the S/R_{quv} -criterion selects a portion of the initial Stokes profiles (dashed-black lines in Figs. 1a-2a) that more closely resembles the original B_{\parallel} distribution (solid-black lines) than profiles selected by the S/R_{qu} -criterion (dashed-black lines in Figs. 3a-4a). This is because the S/R_{quv} -criterion selects a much larger sample of Stokes profiles than S/R_{qu} , hence the distribution obtained with the former criterion must more closely resemble the original distribution employed to construct the database of Stokes profiles (solid-black lines).

We also note that the distribution of the component of the magnetic field vector along the observer’s line-of-sight B_{\parallel} is very accurately retrieved by the inversion in all instances, regardless of the selection criterion and either of the noise levels (see Figs. 1a-4a). This conclusion is reached from the fact that solid-red lines coincide almost perfectly with the dashed-black lines in all figures. In addition, the solid-red curves shift towards lower values of B_{\parallel} as the noise decreases, which indicates that lower levels of noise

allow us to correctly infer smaller values of the line-of-sight component of the magnetic field.

4.2. Transverse component of the magnetic field: B_{\perp}

For the same reason given above in the case of B_{\parallel} , the S/R_{quv} -criterion selects a portion of the initial Stokes profiles (dashed-black lines in Figs. 1b-2b) that resembles much more closely the original B_{\perp} distribution (solid-black lines) than profiles selected by the S/R_{qu} -criterion (dashed-black lines in Figs. 3b-4b). In addition, the distribution obtained with the S/R_{qu} -criterion mostly provides information about the large values of the transverse component of the magnetic field ($B_{\perp} \approx 100 - 150$ G), whereas the S/R_{quv} -criterion also selects profiles arising from weak transverse magnetic fields ($B_{\perp} \lesssim 50$ G). The reason for this is that much larger values of B_{\perp} are needed to produce linear polarization profiles above the 4.5σ -level.

The inversion code very reliably retrieves the distribution of B_{\perp} employing the S/R_{qu} -criterion: we note the almost perfect match between the solid-red curves and dashed-black ones in Figs. 3b-4b. However, this is clearly not the case for the S/R_{quv} -criterion, since here the inversion underestimates the original distribution in the region where $B_{\perp} \lesssim 25 - 40$ G (depending on the noise), but overestimates it in the region above this threshold. It is also noteworthy that the results from the inversion of the Stokes profiles selected with the S/R_{quv} -criterion show a Maxwellian-like distribution, where the peak appears progressively at lower values of B_{\perp} as the noise decreases: $B_{\perp}^{\text{peak}} \approx 60$ G (Fig. 1b; $\sigma = 10^{-3}$) and $B_{\perp}^{\text{peak}} \approx 35$ G (Fig. 2b; $\sigma = 3 \times 10^{-4}$). This is a consequence of having a higher sensitivity for lower levels of noise.

4.3. Total magnetic field strength: B

Since $B = \sqrt{B_{\parallel}^2 + B_{\perp}^2}$, and since the inversion of Stokes profiles retrieves very reliable distributions for B_{\parallel} , any mismatch between the original distributions of B (dashed-black) and the inferred ones (solid-blue) in Figs. 1c-4c, can be attributed to the same issues as the inference of B_{\perp} (see above). In particular, as for B_{\perp} , the S/R_{qu} -criteria allows us to retrieve the distribution of the module of the magnetic field vector B reliably, while the S/R_{quv} -criteria underestimates the real distribution for values $B \lesssim 35 - 70$ G (depending on the noise) but overestimates it above this threshold (solid-blue lines in Figs. 1c and 2c).

4.4. Inclination of the magnetic field vector: γ

As happens with B_{\parallel} and B_{\perp} , the S/R_{quv} -criterion selects a set of Stokes profiles (dashed-black lines in Figs. 1d-2d) that are more representative of the initial uniform distribution in γ (solid-black lines) than the Stokes profiles chosen with the S/R_{qu} -criteria (dashed-black lines in Figs. 3d-4d). The S/R_{quv} -criterion selects all sorts of inclinations, with a slight preference for more longitudinal magnetic fields. The S/R_{qu} -criterion selects however only highly inclined

fields ($\gamma \rightarrow 90^\circ$). This happens because for weak magnetic fields, the only way to have linear polarization signals above the 4.5σ -level is for these magnetic fields to be highly inclined. This can also be understood in terms of the kind of distributions obtained in B_{\parallel} and in B_{\perp} (panels **a**) and **b**), respectively) by each selection criteria and remembering that $\gamma = \tan^{-1}(B_{\perp}/B_{\parallel})$.

By comparing the dashed-black and solid-red lines in Figs. 1d-4d, we can conclude that the inversions of the Stokes profiles selected with the S/R_{quv} -criterion yields a distribution of γ that is underestimated for more longitudinal magnetic fields, but overestimated for more transverse ones. We note that the turning point between the underestimation of vertical magnetic fields and the overestimation of horizontal ones occurs at lower values of γ as the noise decreases: $\gamma \simeq 22^\circ$ for $\sigma = 10^{-3}$ but only at $\gamma \simeq 17^\circ$ for $\sigma = 3 \times 10^{-4}$. Interestingly, the probability distribution function around $\gamma = 90^\circ$ (where magnetic fields are perpendicular to the line-of-sight) is reliably inferred with this criterion. Altogether, these findings confirm our previous results (see paper I), for which we concluded that the inversion of the Stokes profiles obtained with the S/R_{quv} -criterion will correctly infer very inclined magnetic fields, whenever these are present, but unfortunately also interpret as very inclined magnetic fields those that are mostly aligned with the observer's line-of-sight. In contrast, the inversion of pixels selected with the S/R_{qu} -criterion retrieves almost perfectly the distribution of the selected pixels, as can be seen by comparing the dashed-black and solid-red curves in Figs. 3d-4d.

4.5. Azimuth of the magnetic field vector: ϕ

Here, both the S/R_{quv} and S/R_{qu} -criteria select a set of Stokes profiles that are representative of the original uniform azimuthal distribution of the magnetic field vector, ϕ , as the selected distributions are also very close to uniform (compare the dashed-black and solid-black lines in Figures 1e-4e).

Remarkably, the inversion of the selected Stokes profiles for both values of the photon noise, σ , and both selection criteria is able to retrieve the original distribution of the selected profiles, as the solid-red lines in Figures 1e-4e match the dashed-black ones. To a first approximation (Auer et al. 1977; Jefferies & Mickey 1991), the azimuthal angle of the magnetic field vector is given by $\phi = (1/2)\tan^{-1}(U/Q)$. Thus, that the inversion of the Stokes profiles selected with the S/R_{quv} -criterion also retrieves the correct distribution for ϕ comes as a rather surprising result, since here most of the selected Stokes Q and U profiles are below the 4.5σ -level (see Section 3). We address this particular point in Section 5.

4.6. Magnetic filling factor: α

In the case of the magnetic filling factor α , neither the S/R_{quv} nor the S/R_{qu} criteria (dashed-black lines in Figs. 1f-4f) are able to recover correctly the original uniform distribution (solid-black lines). In particular, most

of the Stokes profiles arising from low values of the filling factor, $\alpha \lesssim 0.4$, are neglected by both selection criteria. This is because the polarization signals scale linearly with α (see Equation 6) and therefore, small values of the magnetic filling factor yield polarization signals that are below the threshold employed in the selection. The situation is aggravated in the case of S/R_{qu} (Figs. 3-4), where even larger values of α are needed owing to Stokes Q and U being intrinsically smaller than Stokes V .

As far as the inversion is concerned, it is clear that the distribution of the magnetic filling factor of the selected profiles is very well-retrieved (solid-red lines in Figs. 1f-4f) for both noise levels and when employing both selection criteria. Interestingly, as happened with γ (although to a much smaller extent), the inversion code slightly overestimates the selected distribution (dashed-black) for $\alpha \lesssim 0.5$, but underestimates it above this value.

We have so far only discussed the ability of the inversion code to retrieve the correct distribution for the magnetic parameters (three components of the magnetic field vector and filling factor). Although this is clearly an important question, it does not provide much information about the reliability of the inversion in individual cases. To address this point, we display in circles in Figure 5, the mean value of the differences between the original physical parameters of the selected Stokes profiles and the inferred ones through the inversion $X^{\text{sel}} - X^{\text{inv}}$. These are denoted as ΔX_i , with X_i being any of the components of \mathbf{X} in Equation 1, which we refer to as *bias* in X_i . In addition to this, we also plot the *standard deviation around the mean* in the inference of the physical parameters as the dashed-color lines, which we refer to as σ_x (not to be confused with the photon noise σ). For a physical parameter to be well-constrained, it is important that the mean is centered around zero (otherwise a systematic bias occurs) and that the standard deviation is small.

We note that the size of the intervals in which the bias and standard deviation are calculated is not constant. This happens as a consequence of the lack of profiles in certain ranges. For instance, the S/R_{qu} criterion barely selects profiles arising from a magnetic field vector where $B_{\perp} < 50$ G (see red and yellow circles in Figs. 3b-4b). This makes it necessary to increase the interval of B_{\perp} (around this range) so that a sufficient number of profiles can be employed to obtain a statistically meaningful ΔB_{\perp} and $\sigma_{B_{\perp}}$ (see green and yellow circles in Figure 5b). This is not needed as often in the S/R_{quv} -criterion because it selects many more profiles than the S/R_{qu} -criterion (blue and red circles in Fig. 5b).

By inspection of Figure 5, we note that, for the same level of noise and with the exception of the magnetic filling factor α , the standard deviation in the retrieval of the physical parameters is always much smaller when employing the S/R_{qu} -criterion than the S/R_{quv} -criterion. By comparing the standard deviations with different levels of photon noise, we realize that for most physical parameters, the improvement achieved by a decrease in the photon noise (from $\sigma = 10^{-3}$ to 3×10^{-4}) is smaller than the improvement achieved by using the S/R_{qu} instead of the S/R_{quv} -criterion. This, generally makes the

dashed-green curves ($\sigma = 10^{-3}$ and S/R_{qu} -criterion) lie below the red-dashed ones ($\sigma = 3 \times 10^{-4}$ and S/R_{quv} -criterion). Interestingly, this does not apply to all physical parameters: in the case of B_{\parallel} and α , the photon noise plays a more important role than the selection criteria itself, as the red curves lie below the green ones. The relative importances of the selection criteria and the photon noise logically depends on the values of the noise considered, thus we cannot conclude that in general the former is more important than the latter (or the other way around) for some particular physical parameter.

We now discuss the errors in the case of the S/R_{quv} -criterion. Here, the retrieval of B_{\perp} (blue and red colors in Fig. 5b) has a large systematic bias towards $B_{\perp}^{\text{inv}} > B_{\perp}^{\text{sel}}$, such as $\Delta B_{\perp} < -75$ G, for $B_{\perp}^{\text{sel}} \lesssim 50$ G. Furthermore, in this same region, the standard deviation is as large as $\sigma_{B_{\perp}} \approx 20 - 50$ G. These numbers decrease as B_{\perp}^{sel} increases, such that $\Delta B_{\perp} \approx -15$ G and $\sigma_{B_{\perp}} \approx 10$ G for $B_{\perp}^{\text{sel}} > 150$ G. As happened in the case of the distributions in Figs. 1c-4c, the bias and standard deviations in the module of the magnetic field vector B (Figure 5c) mimic those of B_{\perp} (Figure 5b). In the case of B_{\parallel} (blue and red colors in Fig. 5a), both the bias and standard deviation are always quite small < 5 G, owing to the Stokes V profiles typically being much larger than Q and U for the same values of B_{\parallel} and B_{\perp} . For the inclination of the magnetic field vector with respect to the observer's line-of-sight, γ (blue and red colors in Fig. 5d), the bias is systematic towards more inclined magnetic fields: $\Delta\gamma < 0$ if $\gamma^{\text{sel}} < 90^\circ$, but $\Delta\gamma > 0$ if $\gamma^{\text{sel}} > 90^\circ$. The absolute value of the bias is indeed larger for magnetic fields aligned with the observer's line-of-sight, where $|\Delta\gamma| \approx 30 - 40^\circ$ if $\gamma^{\text{sel}} \approx 0, 180^\circ$. Interestingly, the bias decreases as the magnetic field vector becomes more perpendicular to the line-of-sight, i.e., $\Delta\gamma = 0$ for $\gamma^{\text{sel}} \approx 90^\circ$. The behavior of σ_{γ} is very similar (at all values) to that of the absolute values of bias $|\Delta\gamma|$. That the bias and standard deviation decrease as $\gamma \rightarrow 90^\circ$ indicates that when the magnetic field vector is not completely aligned with the observer's line-of-sight, the signal that appears in Q and U helps the inversion code to extract some information about the inclination of the magnetic field vector. This inference is however negatively affected by the photon noise systematically overestimating γ . This agrees with our results in paper I, where we found that it was impossible to distinguish between a vertical and horizontal magnetic-field vector when Stokes Q and U are below the 4.5σ -level. Figure 5e displays $\Delta\phi$ and σ_{ϕ} as a function of γ^{sel} instead of ϕ^{sel} . In this case, the bias in the determination of the azimuthal angle of the magnetic field vector is almost negligible for all possible values of γ^{sel} , where $\Delta\phi \approx 0^\circ$. However, the standard deviation is large ($\sigma_{\phi} \approx 40 - 50^\circ$) when the magnetic field vector is aligned with the observer's line-of-sight ($\gamma \rightarrow 0, 180^\circ$), but decreases as the magnetic field vector becomes more and more inclined with respect to the observer's line-of-sight ($\gamma \rightarrow 90^\circ$). This happens as a consequence of the linear polarization profiles vanishing when the magnetic field becomes aligned with the observer such that $Q, U \propto \sin^2 \gamma$ (see Eq. 6).

Compared to the S/R_{quv} -criterion, there is no bias in the retrieval of all parameters (except for the magnetic fill-

ing factor) when employing the S/R_{qu} -criterion $\Delta X_i \rightarrow 0$. In addition, the standard deviation in the retrieval of the physical parameters, σ_x , greatly decreases when employing the S/R_{qu} -criterion, as indicated by the green and yellow colors in Figure 5. With this criterion $\Delta B_{\perp} \approx 0$ G and $\sigma_{B_{\perp}} \approx 10$ G, even for $B_{\perp} < 50$ G. The retrieval of B_{\parallel} also improves, (such that $\sigma_{B_{\parallel}} < 3$ G) from that achieved with the S/R_{quv} -criterion. Finally, this translates into smaller standard deviations for B , γ , and ϕ : $\sigma_B < 5$ G, $\sigma_{\gamma} < 2^\circ$, and $\sigma_{\phi} < 2^\circ$.

5. Can inversion codes retrieve the distribution of the orientation of the magnetic field vector from correlations within the noise ?

5.1. Azimuth of the magnetic field vector: ϕ

In Section 4.5, we have seen that the retrieved distribution of the azimuthal angle of the magnetic field vector on the plane that is perpendicular to the observer's line-of-sight (ϕ) matches excellently well the original uniform distribution for the selected pixels. In the case of the S/R_{quv} -criterion, this seems counter-intuitive since many of the selected Stokes profiles only have sufficient signal in Stokes V , while Q and U are usually dominated by photon noise. One possible explanation for this is that the inversion does not properly infer ϕ but instead yields a random distribution of values owing to the lack of information in the linear polarization profiles. If this distribution happens to be uniformly distributed, then the inferred distribution of azimuths matches the original one, even if the inversion fails for each Stokes vector individually. The second explanation is that, given that the number of profiles with large enough signals in Stokes Q and U is non-negligible, the inversion indeed properly retrieves ϕ . In particular, in Section 3 we mentioned that 21.2 % ($\sigma = 10^{-3}$) and 39.2 % ($\sigma = 3 \times 10^{-4}$) of the profiles selected with the S/R_{quv} -criterion, had linear polarization signals above the 4.5σ -level. A final possible explanation is that the inversion is able to retrieve the correct values of ϕ even when Stokes Q and U are dominated by noise. This could happen if the hidden signal introduces a sufficiently strong correlation in the noise, such that the minimization process can properly retrieve the azimuth of the magnetic field vector. To investigate which of these three possibilities are responsible for our results in Section 4, we repeated the synthesis (Sect. 2) and inversion experiments of the spectral line Fe I 6302.5 Å, but employing the probability distribution function

$$\mathcal{P}_1(\mathbf{B}, \alpha) d\mathbf{B} d\alpha = \frac{1}{\pi B_0} \delta\left(\phi - \frac{\pi}{8}\right) H(B - B_0) dB d\gamma d\phi d\alpha \quad (6)$$

which is very similar to Equation 3 with the exception that the distribution of the azimuthal angle is now a δ -Dirac centered at $22.5^\circ = \pi/8$ rad. This value is chosen such that $Q \propto \sin^2 \gamma \cos 2\phi$, and $U \propto \sin^2 \gamma \sin 2\phi$, have the same amplitudes (see Eq. 6). The distribution given by Equation 6 is employed to produce synthetic Stokes profiles, which are then inverted after adding photon noise with levels of $\sigma = 10^{-3}$ and 3×10^{-4} . The

resulting distributions, for both levels of noise and both selection criteria (S/R_{quv} and S/R_{qu}), are shown in Figure 6.

Figure 6 shows that, on the one hand, the S/R_{quv} -criterion (solid lines) has an almost uniform background distribution. This is caused by the inversion of Stokes profiles whose linear polarization signals are so weak that they carry no information about the azimuth, thus the inversion retrieves random results that happen to be uniformly distributed. We know this because this background uniform field disappears if we apply the S/R_{qu} -criterion (dashed lines), which selects only Stokes Q and U profiles that are 4.5 times above the noise level. This is therefore one of the reasons for the excellent results in Figures 1e-2e.

In Figure 6, the S/R_{quv} -criterion also features (superimposed on the uniform background distribution) a clear reminiscent signature of the original $\delta(\phi - \pi/8)$ distribution (indicated by the vertical black arrow). This indicates that the inversion code is able to retrieve, to some extent, information about the azimuthal angle of the magnetic field vector. However, we still do not know whether ϕ is correctly retrieved in only 21.2/39.2 % ($\sigma = 10^{-3}, 3 \times 10^{-4}$, respectively) of the Stokes profiles that have sufficient signal in the linear polarization or, whether the inversion can properly infer ϕ even when the linear polarization signals are below the 4.5σ -level. To answer this question, we devised a third selection criterion, $S/R_{\text{no-qu}}$, for which we selected all profiles where the linear polarization signals were below the 4.5σ -level. The distribution of ϕ obtained with this criterion (dotted-dashed lines in Figure 6) shows an almost uniform distribution, with a far smaller peak at $\phi = \pi/8$ than before. This indicates that when the signals are dominated by noise, the correlation hidden below the noise does not provide sufficient information about the azimuthal angle of the magnetic field vector.

5.2. Inclination of the magnetic field vector: γ

In paper I, we demonstrated that a magnetic field vector that is aligned with the observer's line-of-sight ($\gamma = 0, 180^\circ$) can be easily confused with a more perpendicular one ($\gamma \approx 90^\circ$) owing to the effect of the photon noise. In that experiment, the signals in the linear polarization were solely due to the photon noise. We did not study whether the inversion code could retrieve useful information about γ from the Stokes Q and U profiles that, in spite of being below the 4.5σ -level, introduce a correlation within the noise. To study this possibility, we carry out a similar experiment to the one we have performed in Section 5.1, but focusing instead on the inclination of the magnetic field vector with respect to the observer's line-of-sight γ . To this end, we prescribe a theoretical distribution of the magnetic field vector in the form

$$\mathcal{P}_1(\mathbf{B}, \alpha) d\mathbf{B} d\alpha = \frac{1}{2\pi B_0} \delta\left(\gamma - \frac{\pi}{4}\right) H(B - B_0) dB d\gamma d\phi d\alpha \quad (7)$$

which is identical to the distribution in Equation 6 but where the roles of ϕ and γ are exchanged. That is, the distribution of the azimuth is now uniform and the

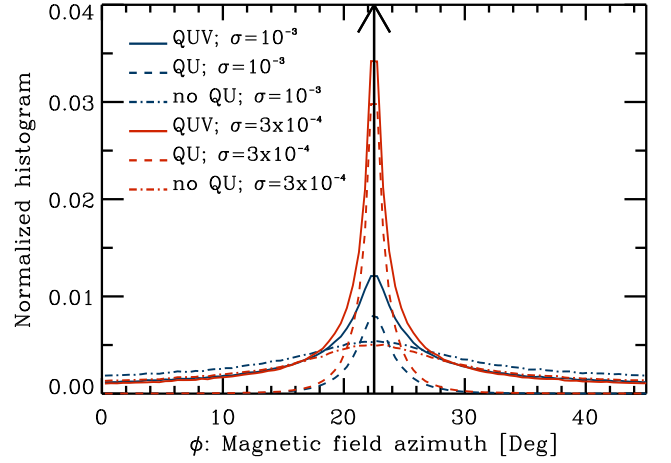


Fig. 6. Histograms of the inferred azimuthal angle of the magnetic field vector, ϕ , when employing Equation 6 in the synthesis of Stokes profiles. The original distribution $\delta(\phi - \pi/8)$ is indicated by the vertical black arrow located at $\phi = 22.5^\circ$. The inferred histograms using S/R_{quv} , S/R_{qu} , and $S/R_{\text{no-qu}}$ criteria are indicated by the solid, dashed, and dotted-dashed lines, respectively. Blue curves are obtained with a photon noise $\sigma = 10^{-3}$, whereas red ones correspond to $\sigma = 3 \times 10^{-4}$.

distribution of the inclination is now a δ -Dirac function centered at $\gamma = 45^\circ = \pi/4$ rad, which is chosen to ensure that $B_{\parallel} = B \cos \gamma$ and $B_{\perp} = B \sin \gamma$ (see Eq. 6) are equal. As we did in Section 5.2, we add to the resulting Stokes profiles synthesized with Equation 7 photon noise with the values $\sigma = 10^{-3}, 3 \times 10^{-4}$. We also apply the three selection criteria mentioned above of S/R_{quv} , S/R_{qu} , and $S/R_{\text{no-qu}}$. The inferred histograms of γ are displayed in Figure 7.

With the first selection criterion, S/R_{quv} , we realize that the inversion code retrieves a distribution of γ (solid lines in Fig. 7) with a clear peak at the original value of $\gamma = 45^\circ$. This distribution has however an extended asymmetric tail towards higher values of γ . This indicates that there is a tendency to retrieve field that are more inclined than they originally are, as a consequence of inverting Stokes profiles where Q and U are not 4.5 times above the noise level. This becomes clear when we consider the S/R_{qu} -criterion (dashed lines in Fig. 7), which ensures that the linear polarization profiles are above the 4.5σ -level, since in this case the tail towards larger values of γ disappears. What are the properties of the peak at $\gamma = 45^\circ$ obtained with the S/R_{quv} -criterion? Is it a consequence of the inversion code being able to properly retrieve the inclination from the weak linear-polarization signals that are below the noise level but introduce a correlation into the noise? Or does the peak contain, as in the case of ϕ (Sect. 5.1) and since a large portion of the Stokes profiles were selected with the S/R_{quv} -criterion, strong linear-polarization signals? This can be answered by the $S/R_{\text{no-qu}}$ -criterion, which only selects Stokes profiles for which Stokes Q and U are below the 4.5σ -level (see dotted-dashed lines in Fig. 7). This selection criteria shows an even more pronounced

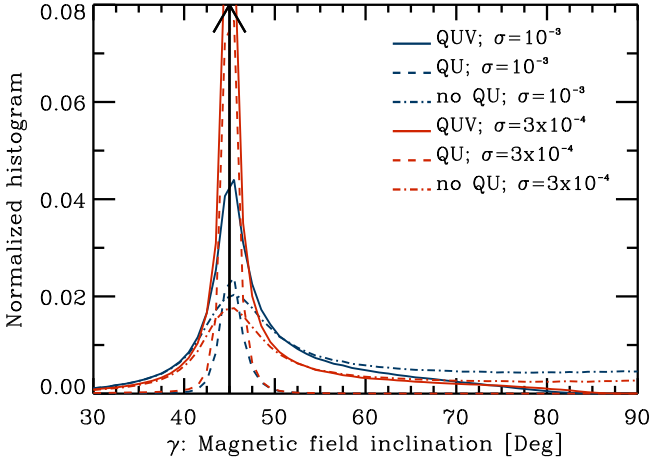


Fig. 7. Histograms of the inferred inclination angle of the magnetic field vector, γ , when employing Equation 7 in the synthesis of Stokes profiles. The original distribution $\delta(\gamma - \pi/4)$ is indicated by the vertical black arrow located at $\phi = 55^\circ$. The inferred histograms using S/R_{quv} , S/R_{qu} , and $S/R_{\text{no-qu}}$ criteria are indicated by the solid, dashed, and dotted-dashed lines, respectively. Blue curves are obtained with a photon noise $\sigma = 10^{-3}$, whereas red ones correspond to $\sigma = 3 \times 10^{-4}$.

tail towards larger values of γ than the S/R_{quv} -criteria. This is a consequence of many more Stokes profiles containing no information about γ owing to very noisy linear-polarization signals. However, the peak at $\gamma = 45^\circ$ does not completely disappear, which indicates that, unlike the case of ϕ , the inversion code is able to partially use the correlation hidden in the noise as a means of determining γ .

We note, however, that this does not mean that the inversion code is able to retrieve the correct distribution of γ by employing the $S/R_{\text{no-qu}}$ -criterion (Stokes Q and U profiles below the 4.5σ -level) when the distribution is a more general one than the δ -Dirac function employed in Equation 7. To emphasize this statement, it suffices to point out that not even the S/R_{quv} -criteria, where 20-40 % of the Stokes profiles have linear polarization signals above the 4.5σ -level, is able to do so (see Figs. 1d-2d). As demonstrated in Section 4, the only way of retrieving the original distributions of the magnetic field vector is to ensure that the linear polarization is above the 4.5σ -level, that is, to apply the S/R_{qu} -criterion.

6. Conclusions

We have carried out several numerical experiments in which a large number of Stokes profiles have been synthesized using uniform distributions of the three components of the magnetic field vector B , γ , and ϕ , and the magnetic filling factor α (Equation 3). To these Stokes profiles, we have added photon noise to two different levels of $\sigma = 10^{-3}$, and $\sigma = 3 \times 10^{-4}$. We have then inverted these profiles in order to retrieve the original distributions employed in the synthesis. This has been done in two different ways. In the first one, we have selected the pixels where the S/R ratio

in any of the polarization signals (circular or linear) are equal to or larger than 4.5, the so-called S/R_{quv} -criterion. In the second case, we have selected the pixels where the S/R ratio in the linear polarization signals is equal to or larger than 4.5, which is the S/R_{qu} -criterion. The former criterion, S/R_{quv} , selects Stokes profiles that arise from all possible ranges of B , γ , and ϕ (dashed-black curves in Fig. 1-2), whereas the S/R_{qu} -criterion selects Stokes profiles that arise from highly inclined magnetic fields (dashed-black curves in Fig. 3-4).

In addition, we have demonstrated (see Section 4) that the S/R_{qu} -criterion can recover, with much larger reliability than S/R_{quv} , the original distributions of the three components of the magnetic field vector from the selected profiles. In particular, the latter criterion clearly overestimates the inclination (with respect to the observer's line-of-sight) of the magnetic field vector γ (solid-red lines in Figs. 1d-2d), and therefore also overestimates the component of the magnetic field that is perpendicular to the observer's line-of-sight, B_\perp (solid-red lines in Figs. 1b-2b). To avoid these systematic errors, we propose employing instead the S/R_{qu} -criterion, which allows the correct distribution of B_\perp and γ (solid-red lines in Figs. 3b,d-4b,d) from the selected profiles to be retrieved. Unfortunately, as mentioned above, the S/R_{qu} -criterion systematically selects the Stokes profiles where the magnetic field vector is already rather inclined, and thus ends up having the same sort of bias as the S/R_{quv} -criterion. It seems therefore that the only way around this problem is to decrease the photon noise to a sufficiently low level that the vast majority of profiles have a S/R ratio larger than 4.5 in the linear polarization profiles. In this way, the selected Stokes profiles would arise from magnetic fields that are representative of the real distribution. It is important to bear in mind that the overestimation of γ and B_\perp is a result that does not depend on the probability distribution function employed in our tests (Eq. 3).

We have also studied the ability of the inversion code to retrieve the angular distribution of the magnetic field vector (γ and ϕ), even when the Stokes Q and U profiles are below the 4.5σ -level (Section 5). In this case, we employed initial distributions of ϕ and γ featuring δ -Dirac functions. We found that the correlation introduced into the noise by these signals does not help us to retrieve the correct azimuthal angle ϕ . Instead of the original δ -function, the inversion code yields a random distribution of azimuthal angles that are uniformly distributed (Fig. 6). In the case of the inclination of the magnetic field vector γ , the inversion code is able to partially retrieve the δ -function from the weak signals below the noise (Fig. 7). However, this is not the case when employing more general distributions, in which case the aforementioned systematic overestimation of γ , dominates the inferred distribution (cf. del Toro Iniesta et al. 2010).

We caution that in our experiments we employed only one spectral line, Fe I ($g_{\text{eff}} = 2.5$) 6302.5 Å, whereas in many previous studies Fe I ($g_{\text{eff}} = 1.67$) 6301.5 Å had also been analyzed. Employing two spectral lines would certainly somewhat improve the results from these experiments as there would be more data points available to the inversion code. However, based on the results of

Orozco Suárez et al. (2010), these improvements will likely be of second order compared to the systematic errors presented in this paper.

An additional point of consideration refers to the numerical code used to infer the magnetic field vector from the inversion of the radiative transfer equation for polarized light (VFISV). This code operates, with some modifications, under a Levenberg-Marquardt non-linear minimization algorithm (Borrero et al. 2010). We cannot exclude that other numerical schemes such as genetic (Lagg et al. 2004) or Bayesian algorithms (Asensio Ramos et al. 2008; Asensio Ramos 2009) are less affected by photon noise and therefore able to infer more accurately the distribution of the magnetic field vector.

Acknowledgements. This research has greatly benefited from discussions that were held at the International Space Science Institute (ISSI) in Bern (Switzerland) in February 2010 as part of the International Working group *Extracting Information from spectropolarimetric observations: comparison of inversion codes*. This work has made use of the NASA Astrophysical Data System.

References

- Asensio Ramos, A., Martínez González, M.J., López Ariste, A., Trujillo Bueno, J. & Collados, M. 2007, ApJ, 659, 829
- Asensio Ramos, A., Trujillo Bueno, J. & Landi Degl’Innocenti, E. 2008, ApJ, 683, 542
- Asensio Ramos, A. 2009, ApJ, 701, 1032
- Auer, L.H., House, L.L. & Heasley, J.N. 1977, Sol. Phys., 55, 47
- Bellot Rubio, L.R. 2003 in: Proceedings of the Solar Polarization Workshop 4. Eds: R. Casini and B.W. Lites. ASP Conf. Series 358, p. 107
- Borrero, J.M., Tomczyk, S., Norton, A., Darnell, T., Schou, J., Scherrer, P., Bush, R. & Liu, Y. 2007, Sol. Phys., 240, 177
- Borrero, J.M., Tomczyk, S., Kubo, M. et al. 2010, Solar Physics, 35
- Borrero, J.M. & Kobel, P. 2011, A&A, 527, 29, paper I
- Domínguez Cerdeña, I., Sánchez Almeida, J. & Kneer, F. 2003, ApJ, 582, 55
- Jefferies, J.T. & Mickey, D.L. 1991, ApJ, 372, 694
- Ishikawa, R. & Tsuneta, S. 2011, ApJ, 735, 74
- Martínez González, M.J., Collados, M. & Ruiz Cobo, B. 2006, A&A, 456, 1159
- Martínez González, M., Asensio Ramos, A., López Ariste, A. & Manso-Sainz, R. 2008, A&A, 479, 229
- Martínez González, M., Manso Sainz, R., Asensio Ramos, A. & Belluzzi, L. 2011, MNRAS, 419, 153
- Mathys, G. 2002 in: Astrophysical Spectropolarimetry, p101-148. Eds: J. Trujillo-Bueno, F. Moreno-Insertis and F. Sánchez. Cambridge University Press. ISBN 0-521-80998-3.
- Lagg, A., Woch, J., Krupp, N. & Solanki, S.K. 2004, A&A, 414, 1109
- Landi Degl’Innocenti, E. 1992 in : Solar Observations, Techniques and interpretations. Eds: F. Sánchez, M. Collados, M. Vázquez. Cambridge University Press, 71.
- Lites, B.W., Leka, K.D., Skumanich, A., Martínez-Pillet, V. & Shimizu, T. 1996, ApJ, 460, 1019
- Lites, B.W., Socas-Navarro, H., Kubo, M. et al. 2007, PASJ, 59, 571
- Lites, B.W., Kubo, M., Socas-Navarro, H. et al. 2008, ApJ, 672, 1237
- López Ariste, A., Martínez González, M.J. & Ramírez Vélez, J.C. 2007, A&A, 464, 351
- Orozco Suárez, D., Bellot Rubio, L.R., del Toro Iniesta, J.C. et al. 2007a, ApJ, 670, L61
- Orozco Suárez, D., Bellot Rubio, L.R., del Toro Iniesta, J.C. et al. 2007b, PASJ, 59, 837
- Orozco Suárez, D., Bellot Rubio, L.R., Vögler, A. & del Toro Iniesta, J.C. 2010, A&A, 518, 2
- Ruiz Cobo, B. 2007 in: Modern solar facilities - advanced solar science, p.287. Eds: F. Kneer, K.G. Puschmann and A.D. Wittmann. ISBN 978-3-938616-84-0.
- Sánchez Almeida, J. 2005, A&A, 438, 727
- Socas-Navarro, H. & Lites, B.W. 2004, ApJ, 616, 587
- Socas-Navarro, H., Borrero, J.M., Asensio Ramos, A. et al. 2008, ApJ, 674, 596
- Stenflo, J.O. 2002 in: Astrophysical Spectropolarimetry, p55-98. Eds: J. Trujillo-Bueno, F. Moreno-Insertis and F. Sánchez. Cambridge University Press. ISBN 0-521-80998-3.
- del Toro Iniesta, J.C. 2003a, AN, 324, 383
- del Toro Iniesta, J.C. 2003b. Introduction to Spectropolarimetry. Cambridge, UK: Cambridge University Press, April 2003. ISBN: 0521818273.
- del Toro Iniesta, J.C., Orozco Suárez, D. & Bellot Rubio, L.R. 2010, ApJ, 711, 312

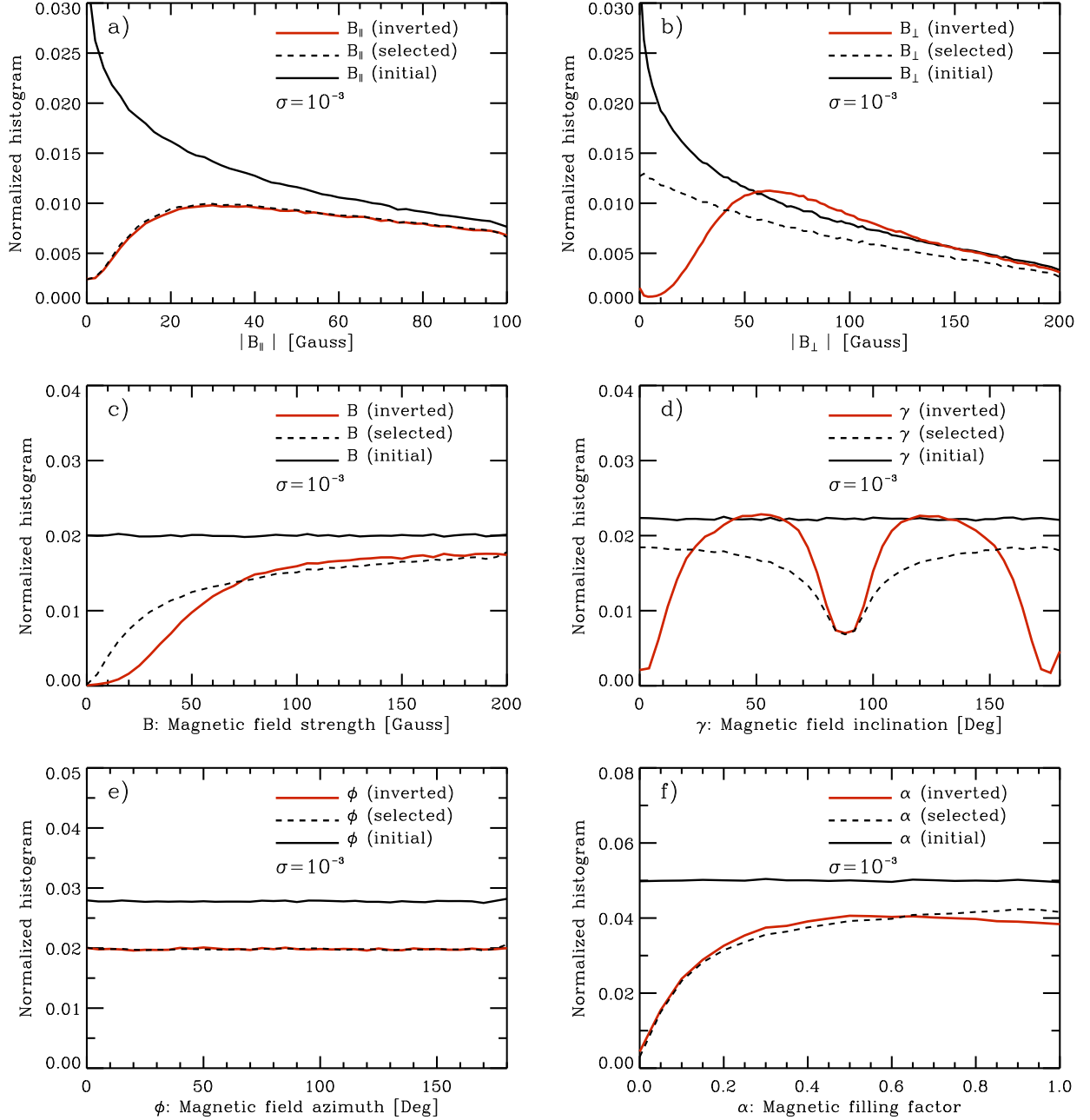


Fig. 1. Results of the numerical experiment of the synthesis and inversion of Stokes profiles. The level noise added is $\sigma = 10^{-3}$. Solid-black lines indicate the original distributions employed in the synthesis of 2×10^6 Stokes profiles (Equation 3). Dashed lines show the distributions obtained employing only the Stokes profiles that are selected with the S/R_{quv} -criterion. The red lines display the distributions obtained from the inversion of the selected profiles: **a)** the absolute value of the component of the magnetic field vector that is parallel to the observer's line-of-sight $|B_{\parallel}| = |B \cos \gamma|$; **b)** the component of the magnetic field vector that is perpendicular to the observer's line-of-sight $B_{\perp} = B \sin \gamma$; **c)** the magnetic field strength or module of the magnetic field vector B ; **d)** the inclination of the magnetic field vector with respect to the observer's line-of-sight γ ; **e)** the azimuthal angle of the magnetic field vector on the plane that is perpendicular to the observer's line-of-sight ϕ ; **f)** the magnetic filling factor α . In all panels, the dashed-black and solid-red curves are normalized to the quotient of the number of profiles selected with each particular criteria to the total number of profiles synthesized (2×10^6).

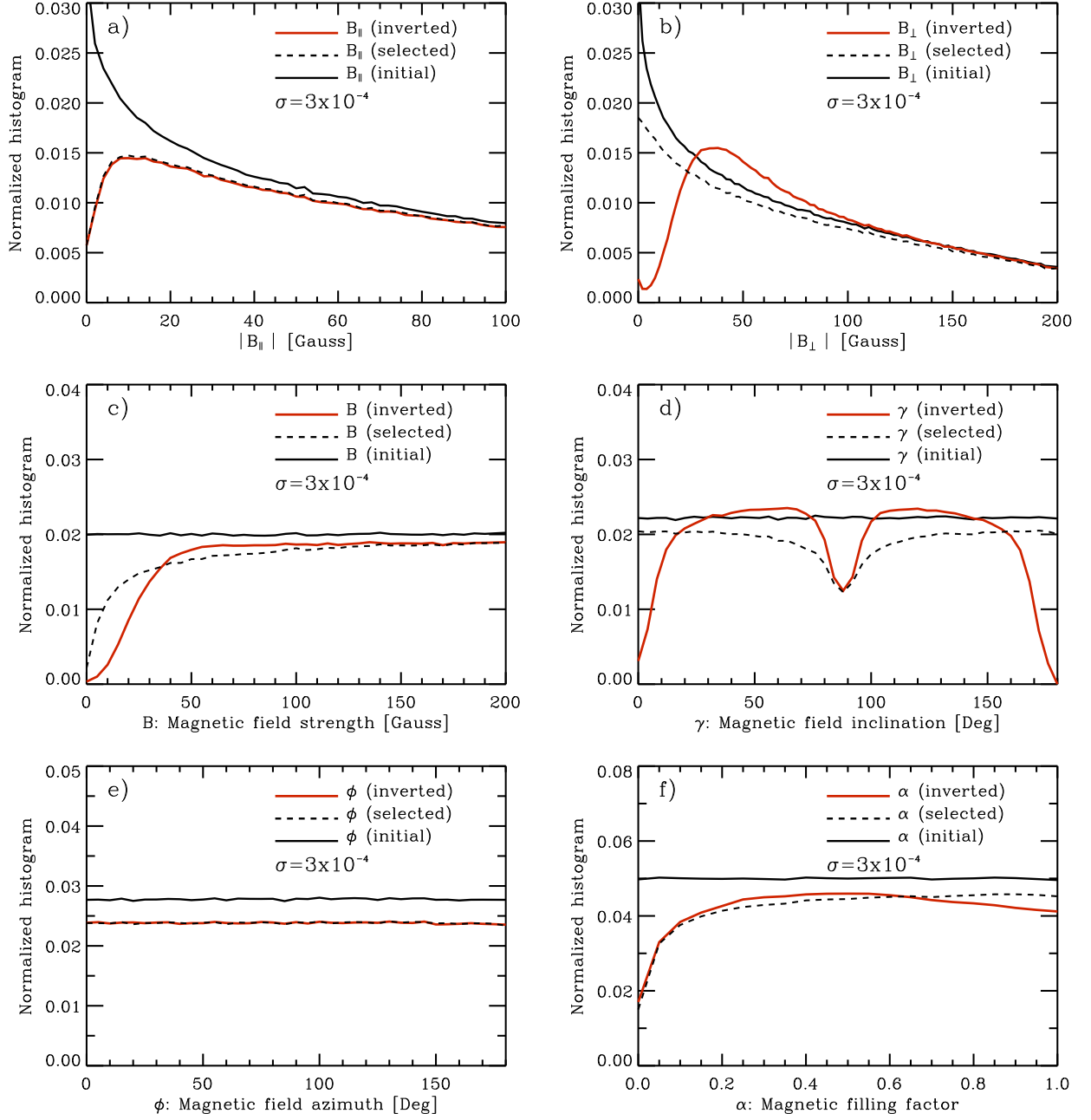


Fig. 2. Same as Figure 1 but using a photon noise $\sigma = 3 \times 10^{-4}$ and the S/R_{quv} -criterion.

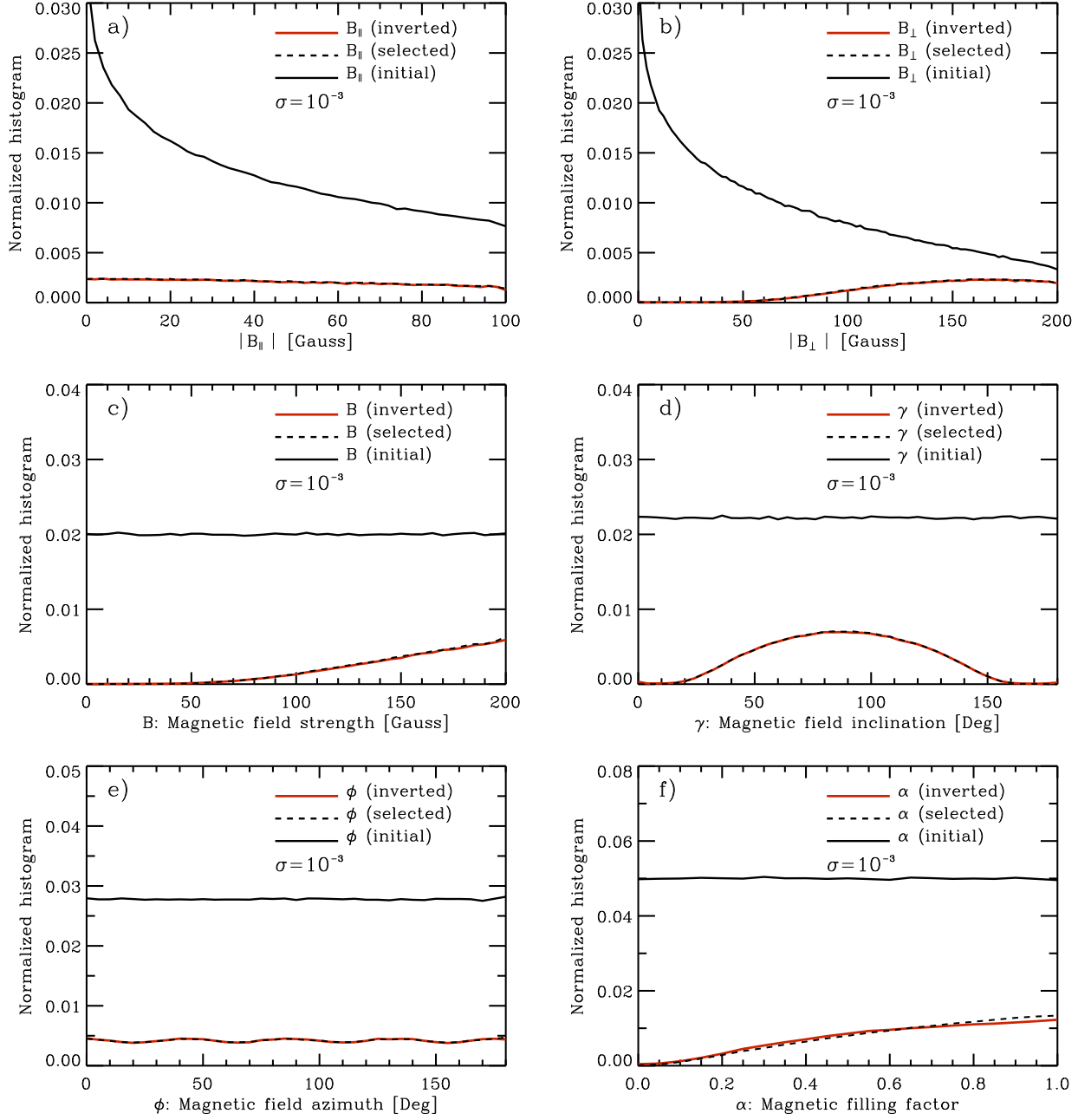


Fig. 3. Same as Figure 1 but using a photon noise $\sigma = 10^{-3}$ and the S/R_{qu} -criterion.

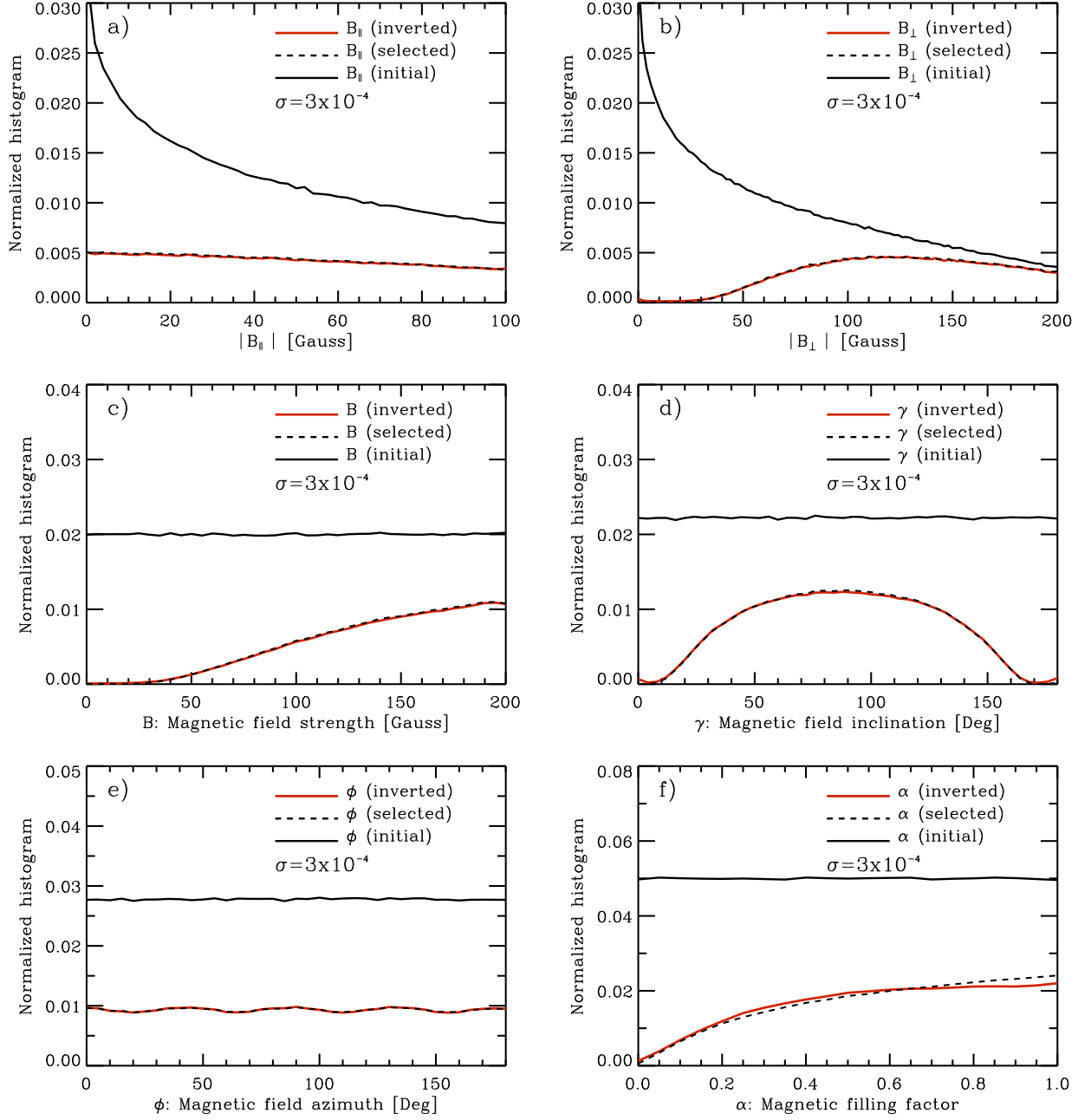


Fig. 4. Same as Figure 1 but using a photon noise $\sigma = 3 \times 10^{-4}$ and the S/R_{qu} -criterion.

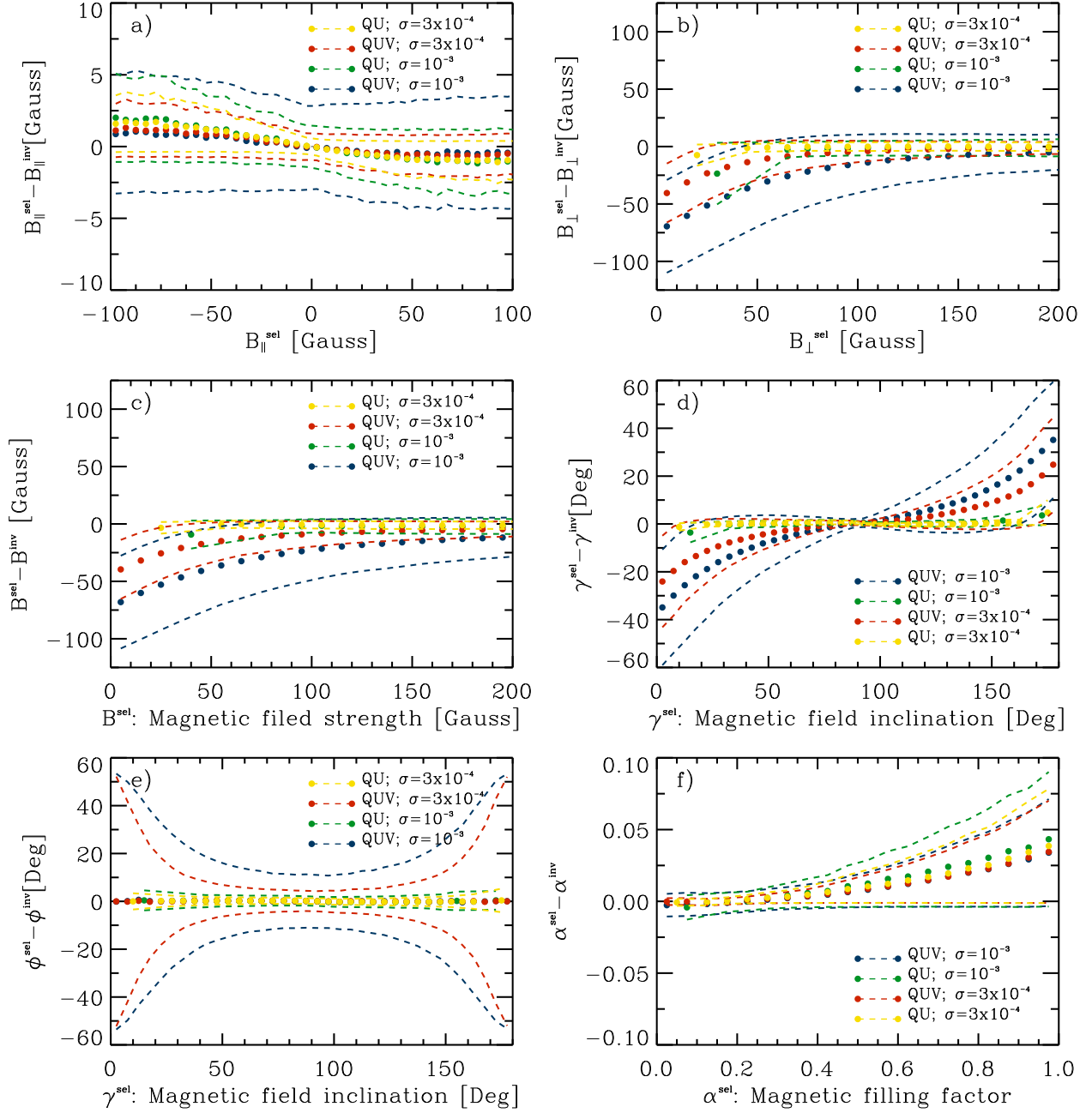


Fig. 5. Mean values of the differences between the original physical parameters and the inferred values (ΔX_i ; circles) and standard deviations around the mean (dashed lines; σ_x): (panel-a) ΔB_{\parallel} and $\sigma_{B_{\parallel}}$ as a function of B_{\parallel} ; (panel-b) ΔB_{\perp} and $\sigma_{B_{\perp}}$ as a function of B_{\perp} ; (panel-c) ΔB and σ_B and a function of B ; (panel-d) $\Delta \gamma$ and σ_{γ} as a function of γ ; (panel-e) $\Delta \phi$ and σ_{ϕ} as a function of γ ; and finally, (panel-f) $\Delta \alpha$ and σ_{α} as a function of α . Blue shows the results obtained from a photon-noise level of $\sigma = 10^{-3}$ and selection criterion S/R_{quv} (from Fig. 1); red represents $\sigma = 3 \times 10^{-4}$ and S/R_{quv} (from Fig. 2); green is for $\sigma = 10^{-3}$ and S/R_{qu} (from Fig. 3); and yellow is for $\sigma = 3 \times 10^{-4}$ and S/R_{qu} (from Fig. 4).